CHEMISTRY OF MATERIALS

Article

pubs.acs.org/cm

Low-Temperature Deposition of Undoped Ceria Thin Films in $scCO_2$ As Improved Interlayers for IT-SOFC

David Mesguich,[†,‡] Cyril Aymonier,*[,‡] Jean-Marc Bassat,*[,‡] Fabrice Mauvy,[‡] Eunyoung You,[†,§] and James J. Watkins*[,†]

[†]Polymer Science and Engineering Department, University of Massachusetts-Amherst, 120 Governors Drive, Amherst, Massachusetts 01003, United States

[‡]CNRS, Université de Bordeaux, ICMCB, 87 avenue du Dr. A. Schweitzer, 33608 Pessac Cedex, FRANCE

[§]Chemical Engineering Department, University of Massachusetts-Amherst, 686 North Pleasant Street, Amherst, Massachusetts 01003, United States

Supporting Information

ABSTRACT: Cerium oxide films were deposited onto various yttria-stabilized zirconia (YSZ) electrolytes using supercritical fluid deposition (SFD) in a cold wall reactor. Deposition of ceria thin films (20−240 nm) was carried out via hydrolysis of a Ce precursor at 250−300 °C (typically 30 min) in supercritical CO_2 ($scCO_2$). The as-deposited films were continuous, dense and crystalline. They exhibited some carbon contamination which was eliminated in all cases by postannealing the films at 400 °C. Film microstructure depends on the hydrolysis conditions (water to cerium molar ratio), on the substrate nature (Si wafers or YSZ pellets) and on the YSZ pellet thickness (100 μm or 1 mm). Ceria films were then used as interlayers for intermediate temperature solid oxide fuel cells (IT-SOFC) between the YSZ electrolyte and the $Nd_2NiO_{4+\delta}$ cathode layer subsequently deposited. The electrochemical properties of the SOFC symmetrical half cells were investigated by electrochemical impedance spectroscopy (EIS). The presence of the undoped ceria layer deposited in $scCO_2$ lowers the resistance of the cell, compared both to cells with an optimized doped ceria layer deposited by screen printing and to cells without any interlayer.

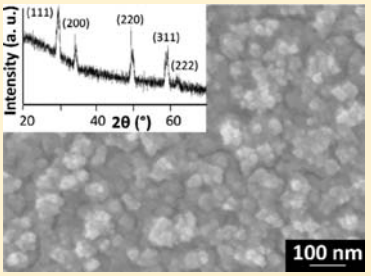

KEYWORDS: *solid oxide fuel cells, undoped ceria interlayer, supercritical fluid deposition, low temperature and conformal deposition, ASR resistance*

INTRODUCTION

Solid oxide fuel cells (SOFC) are high-temperature devices operating around 900−1000 °C. The high temperatures can be advantageous; for example, they enable cogeneration (recovering energy as electricity as well as heat) and internal reforming of the fuel. Unfortunately, such high temperatures also induce high reactivity at the interfaces and high mechanical stress on the cell components, and limit the materials choice, which present significant obstacles for commercialization. Currently, the main challenge is to lower the operating temperature to approximately 600 °C, moving toward intermediate temperature SOFC in an effort to lower the device cost. Lower temperatures allow the use of stainless steel instead of ceramics as interconnects for example, and improve the cells durability and lifetime.[1−4] However, because the electrode reactions and ion transport through the electrolyte are temperature-driven, the electrochemical properties are drastically impaired and new concepts must be developed in order to reach reasonable performance at these intermediate temperatures. In this respect, rare earth doped ceria is a material of high interest for IT-SOFC; its high ionic conductivity (1 order of magnitude higher than state of the art electrolyte YSZ) at 600 °C makes it a suitable electrolyte, as reported more than 30 years ago.[5−7] Partial substitution of the Ce^{4+} ions (typically 10−20%) by trivalent ions (Gd^{3+}, Sm^{3+}, Y^{3+}, etc.) generates oxygen vacancies in the lattice, enabling high oxygen mobility and increasing the ionic conductivity by 1 or 2 orders of magnitude (compared to undoped ceria).[8]

In this work, we focus on the use of ceria as a buffer layer between the cathode and the electrolyte, to prevent cationic chemical diffusion at the interface and to increase the mechanical adherence between YSZ and the cathode, which was recently reported to improve the electrochemical properties of the cells, especially at intermediate temperatures. The microstructure of the ceria layer, which is dependent upon the deposition method, deposition conditions and firing temperature, greatly influences the electrochemical performance of the cells. The use of dense and thin doped ceria layers efficiently prevents cation diffusion while optimizing the oxygen ionic conductivity, leading to improved performance,[9] especially when combined with low-temperature deposition techniques.[10−12]

Typically, SOFC materials are synthesized and deposited in two distinct steps using common ceramic deposition techniques

Received: May 5, 2011
Revised: September 25, 2011
Published: November 23, 2011

such as screen printing of an ink made from a previously obtained powder.[9,11] Mechanical adhesion to the electrolyte and sintering of the deposited layer require a high temperature annealing step (1000−1300 °C). This thermal treatment tends to mitigate the advantages afforded by the various synthesis methods developed to date (such as control of the grain size and morphology). This thermal treatment can also promote chemical diffusion at the interface inducing the formation of unsuitable poorly conductive phases and eventually leads to poor control of the layer microstructure. To overcome these issues, various approaches have been developed to deposit the electrode material or buffer layer directly on top of the electrolyte at a moderate temperature, without the need of a sintering step. Indeed, the deposition of ceria thin films has been increasingly studied these past 10 years using various techniques such as atomic layer deposition (ALD),[13,14] pulsed laser deposition (PLD),[15,16] electron beam evaporation,[12] sputtering,[12,17] chemical vapor deposition (CVD),[18] dip-coating,[19,20] or various spraying techniques[21−25] as detailed in the review of Beckel et al.[26] Such films generally consist of nanosized grains and exhibit very high conductivity. However, in spite of the improvements reported for the electrochemical properties, lengthy deposition times and/or high deposition temperatures (500−750 °C) currently limit the use of most of these techniques. In some cases, additional heat treatments are required to obtain dense and crystalline films.

This paper reports the extension of our surface-selective, cold wall supercritical fluid metal and oxide deposition process to yield conformal nanostructured ceria interlayers (between the cathode and the electrolyte) on low thermal conductivity substrates such as YSZ for application in IT-SOFC. Proof of concept of supercritical fluid deposition of numerous metal and oxide thin films with high deposition rates at relatively low temperatures (from 60 °C up to 300 °C) has been demonstrated on planar and patterned Si substrates.[27−30] In the present study, nanostructured ceria films with film thickness ranging from 20 to 240 nm (and grain size down to 5 nm) have been deposited on various YSZ substrates. Structure, composition, morphology and electrochemical properties of ceria thin films were investigated in relation with substrate nature and thickness, water to ceria precursor molar ratio, temperature, pressure, and deposition time.

EXPERIMENTAL SECTION

The experimental setup and procedure have been previously detailed.[27] Depositions were carried out in a 80 mL cold wall reactor. Deposition in a cold wall reactor is based on independent heating of the reactor walls and of the pedestal on which the substrate is laid to generate a strong temperature gradient between the fluid phase (CO_2) and the substrate surface, leading to precursor decomposition and film formation exclusively onto the substrate. Tetrakis(2,2,6,6-tetramethyl-3,5-heptanedionato) cerium ($Ce(tmhd)_4$) as Ce precursor was supplied by Gelest, Coleman-grade CO_2 (99,99%) was supplied by Merriam Graves, dry nitrogen was supplied in house from a liquid source. First, the substrate was mounted on the heated stage, solid Ce precursor was added, and then the reactor was sealed. After a 1 h nitrogen purge, the reactor was filled with CO_2 and heated up to 60 °C and 10−15 MPa for 1 h in order to soak the Ce precursor ($1-6 \times 10^{-3}$ g/g_{CO_2}). A controlled amount of water (H_2O/Ce molar ratio between 0 and 36) was then added via a sample loop (10, 15, or 50 μL) and the stage temperature was quickly raised to 250−300 °C to initiate the precursor decomposition by hydrolysis leading to film deposition. After 30 min of reaction, heating was turned off leading to the rapid decrease in temperature, effectively ending the reaction. Annealing under air at 400 °C for 6 h was later performed to remove residual carbon in the films.

Ceria films were deposited onto three different substrates: 1 mm thick 8YSZ (8 mol % Y_2O_3) homemade pellets from Tosoh powder pressed and sintered at 1400 °C, and 100 μm thick 8YSZ and 3YSZ (3 mol % Y_2O_3) substrates obtained by tape casting for the preparation of symmetrical half cells (preliminary experiments were carried with silicon wafers as substrates). Ceria films were deposited via SFD in two steps on both sides of YSZ electrolytes. Stainless steel washers were used as masks, leaving a deposition-free zone on the edge of the substrates, to avoid any short-circuit between both sides during electrochemical measurements. A $Nd_2NiO_{4+\delta}$ cathode layer ($Nd_2NiO_{4+\delta}$ powder supplied by Marion Technologies, average particle size = 0.8 μm) was subsequently deposited by screen printing on both sides (20−30 μm thickness) and sintered under air at 1100 °C for 3 h.

Film composition was analyzed by X-ray photoelectron spectroscopy (XPS) using a Quantum 2000 scanning ESCA microprobe (Physical Electronics) coupled with an Ar^+ ion-sputtering gun and charge neutralizing system. Film thickness has been evaluated from XPS sputter depth profiles after calibration with samples of known thickness (see the Supporting Information, part 1). Film crystallinity was characterized by X-ray diffraction (XRD) using PANalytical X'Pert diffractometer (Cu Kα radiation) in 2θ mode with an incident X-ray beam angle fixed at 0.5°, and the detector 2θ angle varying step by step from 20° to 70°. Film morphology was studied by field emission gun scanning electron microscopy (FEG SEM Jeol 6700) under 5.0 kV acceleration voltage.

Symmetrical half cells ($Nd_2NiO_{4+\delta}/CeO_2/YSZ/CeO_2/Nd_2NiO_{4+\delta}$) were characterized by electrochemical impedance spectroscopy (EIS) (Autolab PGSTAT 302N coupled with frequency response analyzer) using a 50 mV signal amplitude and a 0 mV dc bias in the frequency range 1×10^6 to 1×10^{-2} Hz under air between 500 and 800 °C. Platinum grids (mesh 225) mechanically pressed against both electrodes were used as electrical current collectors. Platinum wires were used to connect electrodes to the external electrical circuit. Impedance diagrams were analyzed and fitted using Zview software. Experimental data were compared with reference samples with identical YSZ electrolytes and cathode layers, both with optimized yttria-doped ceria (YDC) layer deposited by screen printing (3−5 μm) and without any interlayer.

RESULTS AND DISCUSSION

Influence of SFD Experimental Conditions on Film Properties. The influence of experimental parameters including precursor concentration, water content, temperature, pressure and deposition time on the properties of ceria films (film morphology, crystallinity and thickness) was determined. The precursor concentration was varied between 1×10^{-3} to 6×10^{-3} g/g_{CO_2}, which ensures that the reaction always took place well below the solubility limit of $Ce(tmhd)_4$ in $scCO_2$ (which is more than 8×10^{-3} g/g_{CO_2} in reaction conditions[31]).

The water content, in relation to the precursor concentration, is a key parameter to control the precursor hydrolysis leading to film deposition, along with the pedestal temperature. These two parameters control the extent of the reaction and thus the film thickness. Additionally, high deposition temperature could enhance film crystallinity and reduce the film carbon content. For our experiments, the water to cerium molar ratio (H_2O/Ce) was varied from zero added water (trace water is present in the CO_2 as used, 10 ppm maximum according to the supplier which corresponds to a water to cerium molar ratio of 0.06 in typical experimental conditions) to 36. The stage temperature was set at 300 °C. This deposition temperature was found sufficient to obtain crystalline films with reasonably

dx.doi.org/10.1021/cm2012846 | Chem. Mater. 2011, 23, 5323−5330

low carbon content. Several experiments were run at 250 °C to evaluate the influence of a lower deposition temperature.

The reaction time was set at 30 min for most depositions. It was also varied for selected experiments, as increasing deposition time (in our case up to 3 h) potentially leads to an increase in film thickness if any unreacted precursor remains. The precursor concentration was varied from 1 to 6 × 10^{-3} g/g_{CO_2} without noticeable effects. The pressure was varied between 13 and 28 MPa, which results in changes in CO_2 density. In all cases the pressure was sufficient to maintain solubility of the precursor and its decomposition products. Experimental conditions for ceria depositions are summarized in Table 1.

Table 1. Experimental Conditions for the Deposition of Ceria Films in $scCO_2$ on Different Substrates[a]

sample name	substrate	H_2O/Ce molar ratio	T (°C)	pressure (MPa)	deposition time
S1_0	8YSZ (100 μm)	0.06	300	18	30 min
S1_11[b]		11		13	
S1_12		12		22	
S1_20		20		22	
S1_36b		36		26	1.5 h
S2_0	8YSZp (1 mm)	0.06	300	18	30 min
S2_11[b]		11		13	
S2_12		12		22	
S2_15		15	250	24	
S2_15b				24	3 h
S2_20		20	300	22	30 min
S2_36b		36		26	1.5 h
S3_12	3YSZ (100 μm)	12	300	22	30 min
S3_27		27		28	
S3_35		35		24	
S3_35b				24	1.5 h

[a]The sample references indicate the substrate used for the deposition (S1, 8YSZ 100 μm thick pellet; S2, 8YSZ 1 mm thick pellet; S3, 3YSZ 100 μm thick pellet) followed by the water to cerium molar ratio. Deposition time is 30 min except for selected experiments carried for longer times, for which the sample reference ends with "b". [b]Soaking temperature of 135 °C instead of 60 °C.

Upon Ce deposition, continuous and uniform films were always obtained. Bright films were obtained on thin YSZ substrates, yet they were not visible on thick YSZ pellets.

XRD data show that the deposited films were well-crystallized and CeO_2 was the only phase detected. Figure 1 shows a representative XRD pattern obtained for ceria thin films deposited on any type of YSZ substrate used in this study. Mild annealing under air (400 °C) was required to eliminate the carbon content of the film (as discussed later); however as-deposited films (before annealing) were always crystalline (see the Supporting Information, part 2). The grain size evaluated using the Debye–Scherrer equation is in the range of 4–6 nm. Interestingly, annealing the samples induces limited grain growth; for instance, for a sample with an initial grain size of 4.1 nm, the grain size is only 4.8 and 5.8 nm after annealing in air for 6 h at 400 and 800 °C, respectively. The SFD process therefore yields films with grain sizes below 10 nm even after annealing, which is significant since when grain size becomes comparable to the dimension of grain boundaries, the

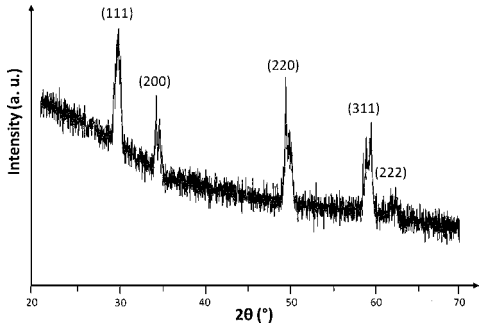

Figure 1. XRD pattern for S2_12; CeO_2 diffraction peaks are indexed (JCPDS 34–0394).

multiplication of interfaces and accumulation of defects can lead to the onset of space charge effects leading to greatly enhanced conductivity.[32–38]

The amount of precursor added and the amount of water injected control the film thickness; increasing the water content promotes the precursor decomposition by hydrolysis leading to higher deposition rate. This study shows the effect of the substrate nature. Indeed YSZ thermal conductivity is 2 orders of magnitude lower than for the Si wafers substrates commonly used (2 and 150 W m^{-1} K^{-1}, respectively). Because the substrates are heated from the bottom by contact with the pedestal, the surface temperature of the electrolyte substrate may be lower than those of bare Si wafers especially as the substrate thickness increases. As the deposition mechanism is temperature-driven, for identical deposition conditions the film thickness is expected to decrease from Si wafers compared to thin and thick YSZ substrates. This has been verified experimentally, for instance, for identical deposition conditions, film thickness decreases from 100 nm for CeO_2 film on Si wafer to 50 nm for S1_12 (100 μm thick YSZ substrate) and only 20 nm for S2_12 (1 mm thick YSZ pellet).

The film surface microstructure was studied using field emission scanning electron microscopy. The results show that the film microstructure depends on the H_2O/Ce molar ratio as well as on the substrate nature. Figure 2 shows the microstructure of ceria films deposited on thin YSZ substrates. The films deposited using high H_2O/Ce molar ratios were smoother and denser (Figures 2e, f) than those deposited in the absence of water (Figures 2b, c). Comparing images c and f in Figure 2, one can see that films deposited in the presence of water offer more uniform coverage and a more regular surface. An additional advantage of the SFD method in comparison with PLD is that SFD yields films comprising small (less than 10 nm), well interconnected grains over the entire range of film thickness studied (20–240 nm). By comparison, columnar growth in PLD yields large grains and ultimately porous structures due to gaps between the grains as film thickness increases.[15,16] Indeed, nanosized grains are visible at high magnification. Similar results were observed for the deposition on Si wafers (see the Supporting Information, part 3). Fracture micrographs (Figure 2d) show a dense, continuous, and uniform deposition several micrometers in length. The substrate surface appears slightly wavy and YSZ grain boundaries remain visible, showing that the deposited ceria films are highly conformal.

However, films deposited onto thick YSZ substrates were smooth for all water concentrations. The films were also conformal and YSZ grain boundaries were still well-defined

dx.doi.org/10.1021/cm2012846 | Chem. Mater. 2011, 23, 5323–5330

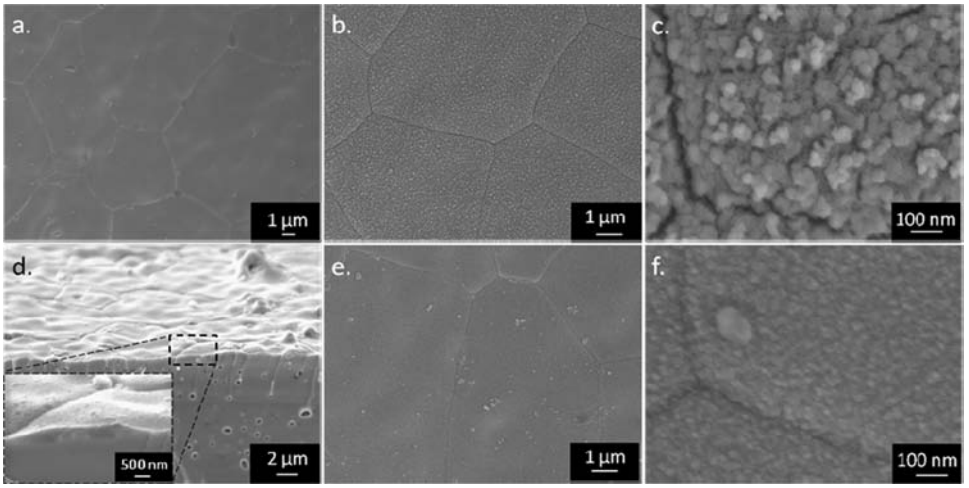

Figure 2. SEM and FEG SEM micrographs of CeO_2 films deposited in $scCO_2$ on 8YSZ (100 μm) substrate without and with water added: (a) substrate surface, (b, c) film S1_0, (d–f) film S1_12. Films annealed at 400 °C.

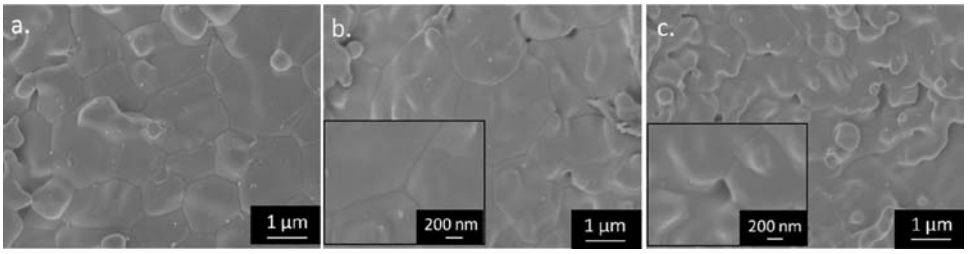

Figure 3. FEG SEM micrographs of CeO_2 films deposited in $scCO_2$ on 8YSZ (1 mm) pellets without and with water added: (a) substrate surface, (b) film S2_0, (c) film S2_12. Films annealed at 400 °C. The insets show higher-magnification images of the films.

(Figure 3). The conformal nature of the ceria films is consistent with previous reports.[27] The SFD technique provides excellent step coverage and conformal deposition within high-aspect-ratio features, which is an advantage over CVD and line-of-sight techniques such as sputtering. The films deposited on YSZ substrates are difficult to image because of the insulating nature of the substrate as well as the weak chemical contrast between the oxide film (CeO_2) and the oxide substrate ($Zr_{1-x}Y_xO_{2-\delta}$). Nonetheless, XRD and XPS data provide ample evidence of ceria deposition on those substrates as well.

The very low thermal conductivity of YSZ substrates could be responsible for the difference in film morphology observed between depositions on thin (100 μm) and thick (1 mm) YSZ substrates. For Si wafers and thin YSZ electrolytes the film morphology depends on water content, suggesting that precursor hydrolysis is governing the deposition process. However, for thicker YSZ substrates the influence of water content on the film morphology is not obvious. In this case, the lower surface temperature may be the primary factor determining the film morphology rather than the water content.

The influence of other experimental parameters on morphology has been evaluated; high soaking temperature (135 °C) leads to thinner films, possibly because of the low thermal stability of $Ce(tmhd)_4$, resulting in its partial decomposition during the soaking step before the reaction step. Therefore a soaking temperature of 60 °C was used as standard. Longer reaction times (3 h instead of 30 min) do not significantly change the film morphology, crystallinity, or composition, which is consistent with high rates of the reaction leading to the film formation.

Figure 4 compares XPS data for film S1_12 before and after annealing at 400 °C. Heat treatment was required to eliminate some carbon impurities in the film, which are likely decomposition products from the cerium precursor, $Ce(tmhd)_4$. After mild annealing, carbon content was systematically below the detection threshold (0.1 at %), the film composition was pure cerium oxide with a uniform Ce concentration. This result is representative of XPS data obtained with all the experiments (including films on Si wafers, see the Supporting Information, part 4).

Determination of Ce oxidation state in the films deposited via SFD is complex. Typical Ce3d XPS profiles (875–920 eV) corresponding to CeO_2 (Ce^{4+}) and Ce_2O_3 (Ce^{3+}) are characteristic, allowing determination of the Ce oxidation state, as previously reported in the literature.[39] Analysis of the XPS data initially suggests that Ce is mainly in Ce^{3+} oxidation state, as reported by O'Neil and Watkins.[27] In fact, the Ce/O atomic ratio of 2/3 shown by sputtering data as well as the characteristic shape of Ce3d peaks support this hypothesis. A closer look at the XPS data shows that for the annealed CeO_2 film as well as for the CeO_2 reference samples (see the Supporting Information, part 5), the first scan (i.e., before sputtering, bottom spectra) is characteristic of Ce^{4+} while all scans recorded after sputtering indicate the predominance of Ce^{3+}. In fact, previous studies have shown that Ar^+ ion bombardment under vacuum during XPS analysis causes preferential oxygen removal,[40] leading to the reduction of Ce^{4+} into Ce^{3+};[39] it is particularly important for nanocrystalline powders[39] and thin films.[41,42] Therefore, the Ce^{3+} predominance observed by XPS does not contradict the film composition, which is CeO_2 as confirmed by XRD, but is

dx.doi.org/10.1021/cm2012846 | Chem. Mater. 2011, 23, 5323–5330

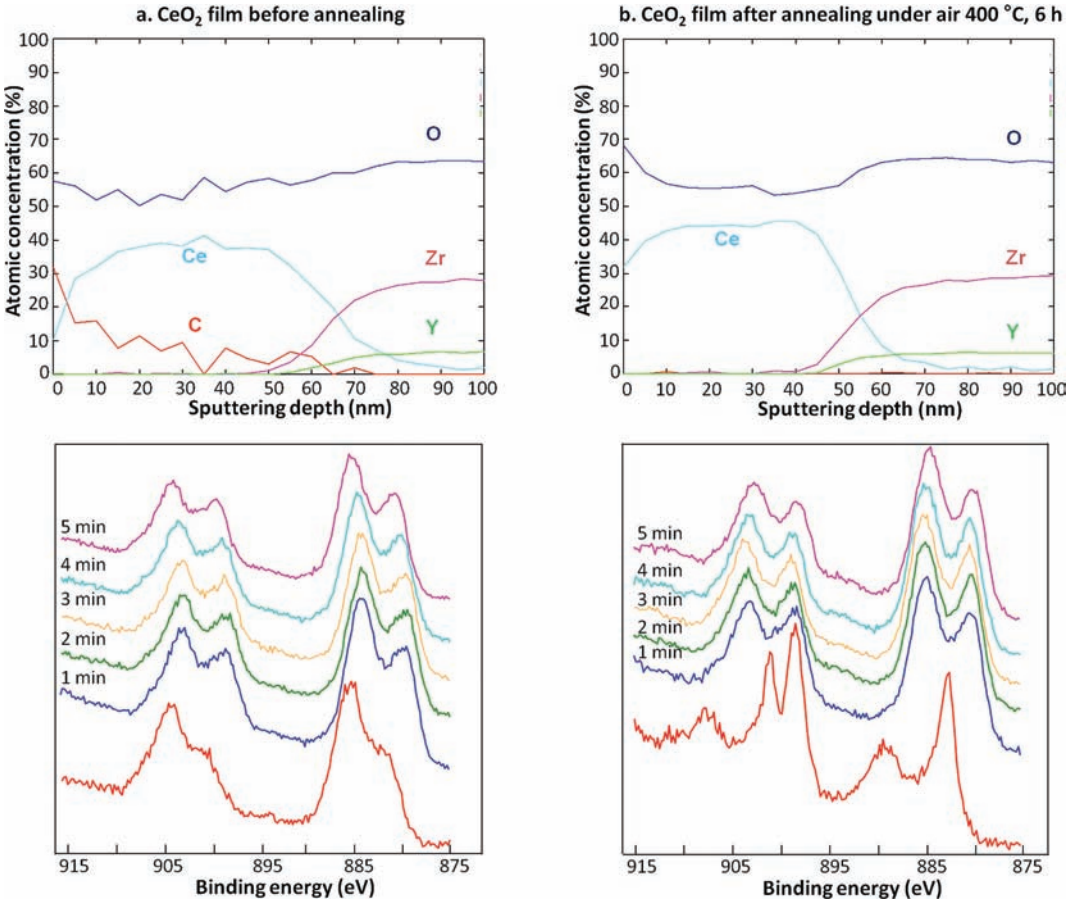

Figure 4. XPS composition profiles and XPS Ce3d profiles after various times of Ar^+ sputtering for film S1_12, (a) before annealing, (b) after annealing under air at 400 °C, 6 h.

most likely due to the reduction caused by Ar^+ ion bombardment of the CeO_2 films during sputtering. However, the first XPS spectra for films before annealing (Figure 4a.) is clearly not characteristic of Ce^{4+}. Surface impurities such as carbon could affect the Ce oxidation state, so conclusions regarding the oxidation state of cerium in films before annealing are difficult.

To summarize, supercritical fluid deposition is a low-temperature technique (300 °C) enabling the formation of crystalline and pure phase CeO_2 films (both before and after annealing) in 30 min, and pure cerium oxide films were obtained after 400 °C annealing. Ceria films are dense and conformal, the film surface reproducing the substrate surface including YSZ grain boundaries. The films also show very good adhesion onto the substrate. More importantly, the water to cerium molar ratio controls both film thickness and film microstructure, which could improve control of the interface for ceria films used as SOFC buffer layers. The combination of two parameters (H_2O/Ce molar ratio and substrate nature) allows tuning of the film microstructure: smooth and dense ceria films were deposited on YSZ thick pellets for any H_2O/Ce ratio and on thin YSZ substrates for high H_2O/Ce ratio (>10) while nanostructured ceria films (composed of nanosized nodules) were deposited on thin YSZ substrates for lower H_2O/Ce ratio. For the matter of film crystallinity or film composition, variations of the experimental parameters in the range of this study do not lead to significant changes in film properties.

Electrochemical Characterizations. Electrochemical impedance spectroscopy (EIS) measurements were performed on half cells made from SFD CeO_2 films deposited on the various YSZ substrates (8YSZ 100 μm thick electrolytes, 8YSZ 1 mm thick pellets and 3YSZ 100 μm thick electrolytes) with $Nd_2NiO_{4+\delta}$ cathode layer screen-printed on top of both sides. Reference samples consist of identical cells (same YSZ electrolytes, identical cathode layer) except the ceria interlayer which is an optimized 3−5 μm yttria-doped ceria layer deposited by screen printing. A reference sample without any ceria interlayer was also used for comparison. Figure 5 presents the ASR values measured for each cell and plotted versus 1000/T.

Table 2 summarizes ASR values at 600 and 700 °C for cells with different ceria interlayers.

One should note that the cells with undoped ceria films deposited by SFD (with the notable exception of devices with a thin 8YSZ substrate, samples noted S1) exhibit lower ASR values than the reference cell without any buffer layer. Furthermore, some of the ASR values obtained match those of reference cells with a yttria-doped ceria layer deposited by screen printing as an optimized interlayer. The lowest ASR obtained at 600 °C with SFD films deposited in optimal conditions (1.64 Ω cm^2 for **S3_35b**, with a 240 nm thick CeO_2 buffer layer on 3YSZ and 1.19 Ω cm^2 for **S2_36b**, with a 100 nm CeO_2 buffer layer on 8YSZ pellet) are lower than those of our reference cells with YDC interlayer. Because an optimization work in cell preparation is still to be carried, these ASR values do not match the best values reported in the

dx.doi.org/10.1021/cm2012846 | *Chem. Mater.* 2011, 23, 5323−5330

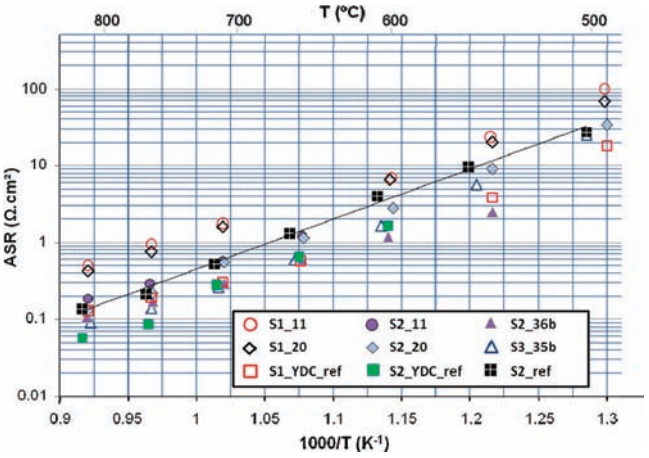

Figure 5. Arrhenius plot of ASR of various cells with different ceria interlayers.

Table 2. ASR Values at 600 and 700 °C for Cells with Different Ceria Interlayers

ceria interlayer	sample name	ASR 600/700 °C (Ω cm²)
undoped ceria thin film deposited by SFD	**S1_11**	6.97/1.76
	S1_20	6.56/1.59
	S2_11	2.80/0.57
	S2_15	2.99/0.56
	S2_15b	2.49/0.28
	S2_20	2.79/0.55
	S2_36b	1.19/0.29
	S3_12	2.16/0.32
	S3_27	2.07/0.28
	S3_35	1.83/0.29
	S3_35b	1.64/0.26
screen-printed yttria-doped ceria layer	**S1_YDC_ref**	2.03/0.31
	S2_YDC_ref	1.64/0.28
reference cell without interlayer	**S2_ref**	4.02/0.52

literature for these kinds of materials (for example see[9]). However, comparing the ASR values measured for cells with SFD undoped ceria buffer layer with our own virtually identical reference cells (except for the screen-printed YDC buffer layer) allows us to draw direct conclusions about the influence of the interlayer in the absence of any other material, deposition method or microstructural differences.

These results are striking, because they imply that an undoped ceria layer can be beneficial to the overall electrochemical properties of SOFC. They clearly demonstrate that the deposition of dense undoped ceria thin films as buffer layers on the electrolyte contributes to the lowering of the ASR. Earlier work on doped ceria films[10−12] suggests that a dense interlayer of a few tens of nanometer contributes to the lowering of the ASR; here we show that this result can be achieved with undoped ceria films, although this material is almost never used for SOFC because of its lower ionic conductivity compared to doped ceria. The well-controlled film thickness as well as the grain size in the nanometer range enabled by the SFD technique probably promote the formation of defects in the ceria lattice enhancing the conductivity. Moreover the low temperature deposition of dense crystalline ceria films should lead to a different interface with the cathode (compared to traditional techniques including high temperature sintering of porous layers), which could be responsible for the improvement of the electrochemical properties. The space charge model predicts a vast improvement of the conductivity at the nanometer scale[33,34,38] which has been experimentally verified, in particular for undoped ceria thin films.[15,35,36] Beyond the change in defect chemistry at the nanometer scale (nanopowders and thin films being easily reducible, they tend to naturally accommodate more oxygen vacancies[43,44]), mechanical properties, and wettability effects could lead to improved transport properties. Providing an intimate interface is of utmost importance for efficient SOFC buffer layers and EIS measurements reported here show that SFD is an interesting low-temperature technique to obtain improved interface facilitating the ionic transfer to achieve better electrochemical performance.

SFD of undoped ceria thin films thus allows fine control of the film properties and microstructure which then influence the performance of the cells. For instance, the substrate may be altered to influence performance. A comparison between films **S1_11** and **S2_11** or **S1_20** and **S2_20**, respectively, shows that in strictly identical conditions, the ASR value was much larger when the ceria film was deposited on 8YSZ 100 μm rather than 8YSZ 1 mm. This result was systematically observed. However, taking a closer look at ASR values for cells with ceria layers deposited on 3YSZ 100 μm electrolytes (samples noted S3) one can see that ceria films deposited on thin substrates can lead to low ASR values. The vast difference observed with thin electrolytes, depending on the electrolyte nature (8YSZ for samples S1 and 3YSZ for samples S3) is likely to be due to a difference in mechanical properties. Zr^{4+} substitution (sometimes referred as "doping") by an aliovalent ion such as Y^{3+} creates oxygen vacancies in the lattice, improving its ionic conductivity; substitution of ZrO_2 with 8 mol % Y_2O_3 stabilizes the cubic fluorine structure of zirconia from room temperature to its melting point. Lower substitution (3 mol % Y_2O_3) stabilizes tetragonal zirconia, which bears better mechanical properties but lower conductivity.[45] Here we assume that the higher thermal expansion coefficient of 3YSZ (compared to 8YSZ, 10.8 and 10.1 K^{-1}, respectively[46]), closer to that of CeO_2 (12.1×10^{-6} K^{-1} [8]), improves the interface between the electrolyte and the interlayer. Mechanical compatibility may be particularly important during the firing step of the cells under air at 1100 °C for 3 h (required to ensure sintering and mechanical adhesion of the cathode layer deposited by screen printing). However, this mismatch in thermal expansion coefficient did not cause any issue when using thick 8YSZ electrolytes because thicker substrates are less subject to warpage behavior at high temperatures. This mechanical issue with thin substrates could be avoided by changing the cathode deposition method, for example. We underline that film adhesion of ceria on all YSZ substrates was very good after deposition and after annealing at 400 °C as evidenced by simple scotch tape tests.

EIS measurements show that the best results were obtained when the ceria interlayer was deposited on the electrolyte with a high H_2O/Ce molar ratio (around 30); this was verified for all the electrolytes used in this study. Comparison of ASR values for the cells with interlayers deposited on thin 3YSZ, **S3_12**, **S3_27**, and **S3_35**, shows a continuous reduction of the ASR value when the water to cerium ratio increases from 12 to 27 to 35, respectively. The same trend was observed with ceria films

dx.doi.org/10.1021/cm2012846 | *Chem. Mater.* 2011, 23, 5323−5330

deposited on thick 8YSZ electrolytes, the ASR value decreasing when H_2O/Ce molar ratio increases from 15 to 20 and 36 for films **S2_15**, **S2_20**, and **S2_36b**, respectively.

Varying the deposition temperature between 250 and 300 °C does not influence the overall ASR (comparison between **S2_15** and **S2_20** for example), which can be expected because it does not change significantly the deposition kinetics or film thickness. Increasing the reaction time for depositions at 300 °C (from 30 min up to 1 h 30 min, **S3_35** and **S3_35b**) does not provoke significant variations of the electrochemical properties, whereas it leads to a slight diminution of the corresponding cell ASR value when deposition occurs at 250 °C (from 30 min to 3 h, **S2_15** and **S2_15b**). It is worth noting that the effect of longer reaction time seems more important when dealing with 1 mm thick YSZ substrates, which is consistent with the hypothesis of lowered reaction kinetics limiting the deposition on thick substrates.

CONCLUSION

Crystalline ceria films free of carbon contamination (after annealing in air at 400 °C) have been deposited on different YSZ electrolytes using $scCO_2$. A very short deposition time (30 min) associated with moderate temperatures (300 °C) allows the deposition of dense ceria thin films on various types of YSZ substrates. Films were in all cases continuous and conformal (YSZ grain boundaries are still visible after deposition). Thickness (20−240 nm) and micro/nanostructure of the films vary depending on the H_2O/Ce molar ratio and the thickness of YSZ substrate. Finally, films always exhibit an excellent adhesion to the substrate, regardless of its nature. Film deposition was uniform and the morphology was homogeneous on the micrometer scale. At smaller scale, regardless of the type of YSZ substrate, electrolyte grain boundaries are always visible after film deposition, which indicates excellent coverage of the substrate with an identical thickness at all points to reproduce the roughness of the substrate.

Such undoped ceria films deposited via SFD were used as interlayers for SOFC, between a YSZ electrolyte and a $Nd_2NiO_{4+\delta}$ cathode. ASR values lower than those corresponding to reference cells with YDC interlayer have been reached (1.19 Ω cm^2 at 600 °C) which demonstrate both the utility of the technique and the potential use of nanostructured undoped ceria thin films for SOFC application.

We are now extending the study to the deposition of doped ceria films via SFD in $scCO_2$, as this is the material commonly used as an interlayer for SOFCs. Simple codeposition of the dopant and ceria proved unsuccessful due to significant differences in the deposition rates from useful precursors. We recently developed a new approach for mixed oxide and doped oxide film depositions from CO_2 that uses alternating precursor flows to remedy this situation.[47]

ASSOCIATED CONTENT

Supporting Information

Additional figures and information (PDF). This material is available free of charge via the Internet at http://pubs.acs.org.

AUTHOR INFORMATION

Corresponding Author

*Phone: +33 5 40 00 26 72 (C.A.); +33 5 40 00 27 53 (J.-M.B.); +1 413 545 2569 (J.J.W.). E-mail: aymonier@icmcb-bordeaux.cnrs.fr (C.A.); bassat@icmcb-bordeaux.cnrs.fr (J.-M.B.); watkins@polysci.umass.edu (J.J.W.).

ACKNOWLEDGMENTS

We gratefully acknowledge funding from the NSF through the Center for Hierarchical Manufacturing at the University of Massachusetts (CMMI-0531171) and the French Ministry of Higher Education and Research.

REFERENCES

(1) Huijsmans, J.; van Berkel, F.; Christie, G. *J. Power Sources* **1998**, *71*, 107−110.
(2) Ralph, J. M.; Schoeler, A. C.; Krumpelt, M. *J. Mater. Sci.* **2001**, *36*, 1161−1172.
(3) Steele, B. C. H.; Heinzel, A. *Nature* **2001**, *414*, 345−352.
(4) Molenda, J.; Swierczek, K.; Zajac, W. *J. Power Sources* **2007**, *173*, 657−670.
(5) Tuller, H. L.; Nowick, A. S. *J. Electrochem. Soc.* **1975**, *122*, 255−259.
(6) Dalslet, B.; Blennow, P.; Hendriksen, P.; Bonanos, N.; Lybye, D.; Mogensen, M. *J. Solid State Electrochem.* **2006**, *10*, 547−561.
(7) Kharton, V. V.; Figueiredo, F. M.; Navarro, L.; Naumovich, E. N.; Kovalevsky, A. V.; Yaremchenko, A. A.; Viskup, A. P.; Carneiro, A.; Marques, F. M. B.; Frade, J. R. *J. Mater. Sci.* **2001**, *36*, 1105−1117.
(8) Mogensen, M.; Sammes, N. M.; Tompsett, G. A. *Solid State Ionics* **2000**, *129*, 63−94.
(9) Ferchaud, C.; Grenier, J.-C.; Zhang-Steenwinkel, Y.; van Tuel, M. M.; van Berkel, F. P.; Bassat, J.-M. *J. Power Sources* **2011**, *196*, 1872−1879.
(10) Jordan, N.; Assenmacher, W.; Uhlenbruck, S.; Haanappel, V.; Buchkremer, H.; Stöver, D.; Mader, W. *Solid State Ionics* **2008**, *179*, 919−923.
(11) Mai, A.; Haanappel, V. A.; Tietz, F.; Stöver, D. *Solid State Ionics* **2006**, *177*, 2103−2107.
(12) Uhlenbruck, S.; Jordan, N.; Sebold, D.; Buchkremer, H.; Haanappel, V.; Stöver, D. *Thin Solid Films* **2007**, *515*, 4053−4060.
(13) Päiväsaari, J.; Putkonen, M.; Niinistö, L. *J. Mater. Chem.* **2002**, *12*, 1828−1832.
(14) Ballé, E.; Ringuedé, A.; Cassir, M.; Putkonen, M.; Niinistö, L. *Chem. Mater.* **2009**, *21*, 4614−4619.
(15) Chmielowska, M.; Villain, S.; Kopia, A.; Dallas, J.; Kusinski, J.; Gavarri, J.; Leroux, C. *Thin Solid Films* **2008**, *516*, 3747−3754.
(16) Pryds, N.; Rodrigo, K.; Linderoth, S.; Schou, J. *Appl. Surf. Sci.* **2009**, *255*, 5232−5235.
(17) Brahim, C.; Ringuedé, A.; Gourba, E.; Cassir, M.; Billard, A.; Briois, P. *J. Power Sources* **2006**, *156*, 45−49.
(18) Suh, S.; Guan, J.; Miinea, L. A.; Lehn, J.-S. M.; Hoffman, D. M. *Chem. Mater.* **2004**, *16*, 1667−1673.
(19) Avellaneda, C. O.; Berton, M. A.; Bulhões, L. O. *Sol. Energy Mater. Sol. Cells* **2008**, *92*, 240−244.
(20) Piñol, S.; Morales, M.; Espiell, F. *J. Power Sources* **2007**, *169*, 2−8.
(21) Gallage, R.; Matsuo, A.; Watanabe, T.; Matsushita, N.; Yoshimura, M. *J. Electroceram.* **2009**, *22*, 33−39.
(22) Lin, H.; Ding, C.; Sato, K.; Tsutai, Y.; Ohtaki, H.; Iguchi, M.; Wada, C.; Hashida, T. *Mater. Sci. Eng., B* **2008**, *148*, 73−76.
(23) Rupp, J. L. M.; Drobek, T.; Rossi, A.; Gauckler, L. J. *Chem. Mater.* **2007**, *19*, 1134−1142.
(24) Song, H. Z.; Wang, H. B.; Zha, S. W.; Peng, D. K.; Meng, G. Y. *Solid State Ionics* **2003**, *156*, 249−254.
(25) Taniguchi, I.; Hosokawa, T. *J. Alloys Compd.* **2008**, *460*, 464−471.
(26) Beckel, D.; Bieberle-Hütter, A.; Harvey, A.; Infortuna, A.; Muecke, U.; Prestat, M.; Rupp, J.; Gauckler, L. *J. Power Sources* **2007**, *173*, 325−345.
(27) O'Neil, A.; Watkins, J. *Chem. Mater.* **2007**, *19*, 5460−5466.
(28) Blackburn, J.; Long, D.; Cabañas, A.; Watkins, J. *Science* **2001**, *294*, 141−145.

(29) Romang, A. H.; Watkins, J. J. *Chem. Rev.* **2010**, *110*, 459−478.
(30) Cansell, F.; Aymonier, C. *J. Supercrit. Fluids* **2009**, *47*, 508−516.
(31) Andersen, W. C.; Sievers, R. E.; Lagalante, A. F.; Bruno, T. J. *J. Chem. Eng. Data* **2001**, *46*, 1045−1049.
(32) Kim, S.; Maier, J. *J. Electrochem. Soc.* **2002**, *149*, J73−J83.
(33) Tschöpe, A. *Solid State Ionics* **2001**, *139*, 267−280.
(34) Tschöpe, A.; Birringer, R. *J. Electroceram.* **2001**, *7*, 169−177.
(35) Kosacki, I.; Suzuki, T.; Petrovsky, V.; Anderson, H. U. *Solid State Ionics* **2000**, *136*−*137*, 1225−1233.
(36) Suzuki, T.; Kosacki, I.; Anderson, H. U. *Solid State Ionics* **2002**, *151*, 111−121.
(37) Lavik, E. B.; Kosacki, I.; Tuller, H. L.; Chiang, Y.-M.; Ying, J. Y. *J. Electroceram.* **1997**, *1*, 7−14.
(38) Kim, S.; Maier, J. *J. Eur. Ceram. Soc.* **2004**, *24*, 1919−1923.
(39) Holgado, J. P.; Alvarez, R.; Munuera, G. *Appl. Surf. Sci.* **2000**, *161*, 301−315.
(40) Qiu, L.; Liu, F.; Zhao, L.; Ma, Y.; Yao, J. *Appl. Surf. Sci.* **2006**, *252*, 4931−4935.
(41) Holgado, J. P.; Munuera, G.; Espinós, J. P.; González-Elipe, A. R. *Appl. Surf. Sci.* **2000**, *158*, 164−171.
(42) Chadwick, D.; McAleese, J.; Senkiw, K.; Steele, B. C. H. *Appl. Surf. Sci.* **1996**, *99*, 417−420.
(43) Zec, S.; Boskovic, S.; Kaluderovic, B.; Bogdanov, Z.; Popovic, N. *Ceram. Int.* **2009**, *35*, 195−198.
(44) Zhou, Y.; Rahaman, M. N. *Acta Mater.* **1997**, *45*, 3635−3639.
(45) Ghatee, M.; Irvine, J. *Int. J. Hydrogen Energy* **2010**, *35*, 9427−9433.
(46) Hayashi, H.; Saitou, T.; Maruyama, N.; Inaba, H.; Kawamura, K.; Mori, M. *Solid State Ionics* **2005**, *176*, 613−619.
(47) Le Trequesser, Q.; Mesguich, D.; You, E.; Aymonier, C.; Watkins, J. J.; *J. Supercrit. Fluids,* DOI: 10.1016/j.supflu.2011.11.018.